

Boson sampling discrete solitons by quantum machine learning

Claudio Conti^{1,2,3,*}

¹*Department of Physics, University Sapienza, P.le Aldo Moro 5, 00185 Rome, Italy*

²*Institute for Complex Systems, National Research Council (ISC-CNR), Via dei Taurini 19, 00185 Rome, Italy*

³*Centro Ricerche Enrico Fermi (CREF), Via Panisperna 89a, 00184 Rome, Italy* [†]

(Dated: October 26, 2021)

We use a neural network variational ansatz to compute Gaussian quantum discrete solitons in an array of waveguides described by the quantum discrete nonlinear Schrödinger equation. By training the quantum machine learning model in the phase space, we find different quantum soliton solutions varying the number of particles and interaction strength. The use of Gaussian states enables measuring the degree of entanglement and the boson sampling patterns. We compute the probability of generating different particle pairs when varying the soliton features and unveil that bound states of discrete solitons emit correlated pairs of photons. These results may have a role in boson sampling experiments with nonlinear systems and in developing quantum processors to generate entangled many-photon nonlinear states.

The quantum properties of solitons, self-localized solutions of nonlinear wave equations, inspired fundamental experimental investigations, as optical quantum non-demolition, squeezing [1–4] and photon bound states [5]. Many authors reported on theoretical studies on the quantum features of solitons, as evaporation, breathing and entanglement [6–11]. However, quantum solitons are overlooked in quantum technologies, as their theoretical treatment requires specialized methodologies [12–16] that do not appear compatible with modern quantum information. On the other hand, quantum optical protocols mainly employ linear circuits, and one can argue if nonlinear waves may have a role in quantum computing [17–21], or –reciprocally– if quantum processors may be used to generate quantum solitons. An intriguing opportunity arises from the fact that circuits for the quantum advantage in boson sampling [22–27] adopt the same devices used to observe discrete optical solitons [28–30]. So, can we do boson sampling with solitons?

To merge solitons and quantum information, we need novel methodologies for executing quantum protocols on many-body states bounded by nonlinearity. Recently, neural network (NN) variational ansatzes have been introduced to study quantum many-body models and quantum circuits [31]. Quantum machine learning (QML), i.e., the development of models and training of parametrized quantum circuits [32–36], is a novel successful technique to compute high-dimensional ground states [37]. Hence, QML seems a promising tool in nonlinear quantum optics too.

Here we show that QML in the phase-space allows a comprehensive quantum description of discrete solitons in waveguide arrays. We demonstrate that a trainable boson sampling quantum processor [38, 39] can synthesize various self-localized soliton solutions. Also, bound-states of discrete solitons exhibit entanglement, and QML can be used to compute boson sampling pattern probability that reveal that they generate correlated photons. These results may open the way to a variety of new ex-

periments with nonlinear quantum discrete waveguide arrays, and to the use of solitons as building blocks for quantum information.

Figure 1 shows the boson sampling quantum processor to synthesize quantum lattice solitons in a discrete array with n sites. The circuit is composed by n squeezers with complex squeezing parameters ζ_j , and displacement operators with complex displacements δ_j , being $j = 0, 1, \dots, n-1$ hereafter. A unitary interferometer \hat{U} mixes the modes before entering the waveguide array.

As detailed below, the quantum processor is represented as a neural network in the phase-space. All the parameters of the squeezers, displacements, and interferometers are trainable and initialized as random variables.

We refer to the state generated by the quantum circuit as the Boson sampling variational ansatz (BSVA) used in the quantum discrete nonlinear Schrödinger equation (QDNLS)

$$i\partial_t \hat{\psi}_j = (\hat{\psi}_{j+1} + \hat{\psi}_{j-1}) + \gamma \hat{\psi}_j^\dagger \hat{\psi}_j \hat{\psi}_j \quad (1)$$

on a lattice with size n (see Figure 1a). Quantum discrete solitons are localized solutions of the time-independent QDNLS. The Hamiltonian is

$$\hat{H} = - \sum_j \left(\hat{\psi}_j^\dagger \hat{\psi}_{j+1} + \hat{\psi}_j^\dagger \hat{\psi}_{j-1} \right) + \frac{\gamma}{2} \hat{\psi}_j^\dagger \hat{\psi}_j^\dagger \hat{\psi}_j \hat{\psi}_j = \hat{K} + \hat{V} \quad (2)$$

with the potential energy $\hat{V} = \frac{\gamma}{2} \sum_j (\hat{n}_j^2 - \hat{n}_j)$ being $\hat{n}_i = \hat{\psi}_i^\dagger \hat{\psi}_i$, and the kinetic energy $\hat{K} = \sum_{ij} \omega_{ij} \hat{\psi}_i^\dagger \hat{\psi}_j$ being $\omega_{ij} = -\delta_{i,j-1} - \delta_{i,j+1}$ with i, j in $[0, n-1]$ letting $\omega_{0,-1} = \omega_{n-1,n} = 0$, as homogeneous boundary conditions for a finite lattice. The total particle number operator is $\hat{N} = \sum_j \hat{n}_j$.

To build the ansatz as neural network in the phase-space, we represent a n -body state by its complex characteristic function $\chi(\mathbf{x}) = \chi_R(\mathbf{x}) + i\chi_I(\mathbf{x})$ [40, 41]. \mathbf{x} is a real-valued vector with dimension $1 \times N$ with $N = 2n$. For Gaussian states [42]

$$\chi(\mathbf{x}) = e^{-\frac{1}{4} \mathbf{x} \mathbf{g} \mathbf{x}^T + i \mathbf{x} \mathbf{d}} \quad (3)$$

with \mathbf{g} the real covariance $N \times N$ matrix, and \mathbf{d} the real displacement $N \times 1$ vector. In our notation, we omit the symbols of the dot product such that $\mathbf{x}\mathbf{d}$ and $\mathbf{x}\mathbf{g}\mathbf{x}^\top$ are scalars. Letting $\mu, \nu = 0, 1, 2 \dots, N-1$, one has $\langle \hat{R}_\mu \rangle = d_\mu = \left. \frac{\partial \chi}{\partial x_\mu} \right|_{\mathbf{x}=0}$ and $g_{\mu\nu} = \langle (\hat{R}_\mu - d_\mu)(\hat{R}_\nu - d_\nu) \rangle - iJ_{\mu\nu}$ being $\mathbf{J} = \bigoplus_j \begin{pmatrix} 0 & 1 \\ -1 & 0 \end{pmatrix}$. The canonical positions $\hat{q}_j = \hat{R}_{2j}$ and momentum $\hat{p}_j = \hat{R}_{2j+1}$, are organized in the $N \times 1$ operator array $\hat{\mathbf{R}}$. The vacuum state is a Gaussian state with $\mathbf{g} = \mathbf{1}_{N \times N}$ and $\mathbf{d} = \mathbf{0}_{N \times 1}$. From the vacuum, one can generate specific states by unitary operators, as displacement or squeezing. These transform the canonical variables as $\hat{\mathbf{R}} = \mathbf{M}\hat{\mathbf{R}} + \mathbf{d}'$, where the symplectic matrix \mathbf{M} and the vector \mathbf{d}' depend on the specific operator (detailed, e.g., in [42–44]). The characteristic function changes as

$$\tilde{\chi}(\mathbf{x}) = \chi(\mathbf{x}\mathbf{M})e^{i\mathbf{x}\mathbf{d}'} = \chi(\mathbf{x}\mathbf{M})e^{i(\mathbf{x}\mathbf{M})\mathbf{M}^{-1}(\mathbf{d}'+\mathbf{a})} \quad (4)$$

As shown in Fig. 1b, we represent the characteristic function as a NN layer with two real outputs χ_R and χ_I . The χ layer has two inputs: \mathbf{x} , and a auxiliary bias $N \times 1$ vector \mathbf{a} . The bias vector appears at the output as an exponential factor $e^{i\mathbf{x}\mathbf{a}}$. Fig. 1c shows a linear transformation as a NN layer with two inputs \mathbf{x} and \mathbf{a} and two outputs $\mathbf{x}\mathbf{M}$ and $\mathbf{M}^{-1}(\mathbf{d}'+\mathbf{a})$. By this definition, Eq. (4) is a two-layers NN. Figure 1d shows $\tilde{\chi}$ as the “pullback” of the linear layer from the χ layer: the transformation appears on the left of χ .

Given the vacuum state with characteristic function χ , one can build the NN model of an arbitrary state by multiple pullbacks. Figure 1e shows a n -mode squeezed vacuum, followed by the displacement operator and interferometer as multiple pullbacks. Figure 1e is the NN model for the BSVA in Fig. 1a.

We compute the mean value of observable quantities as \hat{H} and \hat{N} as derivatives of the characteristic function computed in phase-space origin $\mathbf{x} = 0$. We have in asymmetric ordering [41]

$$\langle \hat{K} \rangle = \sum_{jk} \omega_{jk} \left[\frac{\partial^2}{\partial \alpha_j \partial (-\alpha_k^*)} \chi(\boldsymbol{\alpha}) - \frac{\delta_{jk}}{2} \chi \right] \Big|_{\boldsymbol{\alpha}=0} \quad (5)$$

where $\boldsymbol{\alpha} = (\alpha_0 \dots \alpha_{n-1}, \alpha_0^* \dots \alpha_{n-1}^*)$, and $\sqrt{2}\alpha_j = x_{2j} + ix_{2j+1}$, and for the interaction term

$$\langle \hat{V} \rangle = \frac{\gamma}{2} \sum_j \frac{\partial^4 \chi}{\partial \alpha_j^2 \partial (-\alpha_j^*)^2} - 2 \frac{\partial^2 \chi}{\partial \alpha_j \partial (-\alpha_j^*)} + \frac{\chi}{2} \Big|_{\boldsymbol{\alpha}=0}. \quad (6)$$

These quantities can be computed by using automatic differentiation on the NN model. However, as we are dealing with a Gaussian state, derivatives can be explicitly computed algebraically by the tensors \mathbf{g} and \mathbf{d} , which speeds up computing and training the model.

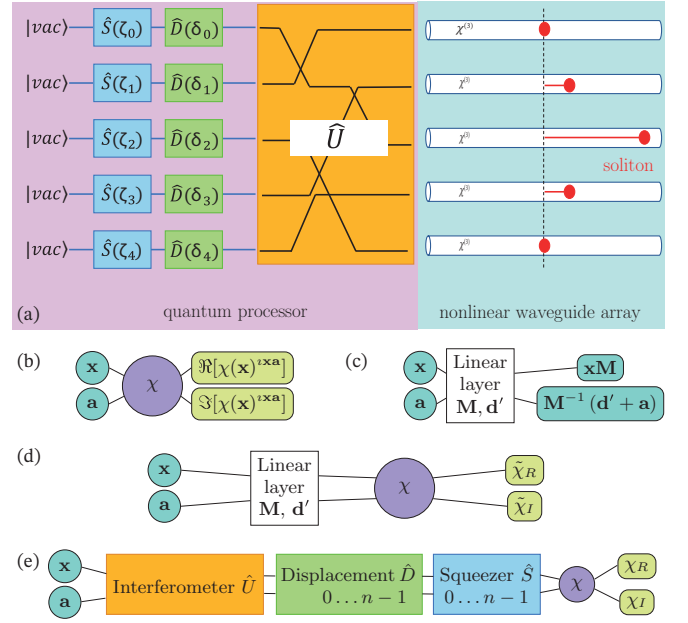


FIG. 1. (a) A boson sampling processor prepares the state to launch the quantum discrete soliton in an array of coupled optical waveguides with cubic $\chi^{(3)}$ nonlinearity. n spatial modes initially in the vacuum state $|\text{vac}\rangle$, are first squeezed and displaced, and then mixed by a trainable interferometer \hat{U} ($n = 5$ in the figure). The state can be represented in the phase space as a quantum neural network that returns the characteristic function χ . (b) The simplest neural network model. Two inputs, a data vector $\mathbf{x}_{1 \times N=2n}$ and a bias vector $\mathbf{a}_{N \times 1}$ seed the model that computes χ and returns the real and imaginary parts of $\chi(\mathbf{x})e^{i\mathbf{x}\mathbf{a}}$. (c) A layer for a linear transformation of the state by a unitary operator represented by a symplectic matrix $\mathbf{M}_{N \times N}$ and displacement vector $\mathbf{d}'_{N \times 1}$. (d) A model representing a state with characteristic function χ , subject to a unitary transformation. This is a pullback of a linear transform from the original state, which produces a new state with characteristic function $\tilde{\chi}$ [see Eq. (4)]. $\tilde{\chi}_R$ and $\tilde{\chi}_I$ are the real and imaginary part of $\tilde{\chi}$. (e) A multiple pullback that represents the many-body state in panel (a). The multiple squeezers and displacements are represented as a single block. Note that the order of the operators, from the vacuum to the interferometer goes from right to left.

Training is done by conventional regression using steepest descent. We use as cost function $\exp(\langle \hat{H} \rangle / n)$, which is minimized as $\langle \hat{H} \rangle < 0$ is at a minimum. As additional cost function, we use $(\langle \hat{N} \rangle - N_T)^2$, to constraint the target boson number $\langle \hat{N} \rangle = N_T$.

Single soliton solution — The classical DNLS is known to admit single solitons with the field localized in one, or two sites as $\gamma < 0$. We want to understand if the trained BSVA can represent quantum version of the single soliton solution. The soliton is found after training the NN model which minimizes the cost function, and the expected Hamiltonian $\langle \hat{H} \rangle$ at fixed $\langle \hat{N} \rangle = N_T$.

We first consider small interaction strength $|\gamma|$, at which we expected delocalized solutions. We show in

Fig. 2a the profile of the expected values for the displacements $|\langle \psi_j \rangle|^2 = (d_{2j}^2 + d_{2j+1}^2)/2$ after the training, and in Fig. 2b the profile of the expected number of bosons per site $\langle \hat{n}_j \rangle$. These profiles are obtained for $N_T = 10$ and $\gamma = -0.01$ after training the model for thousands of epochs.

Strong localization is obtained for for $N_T = 10$ and $\gamma = -1$ as in Fig. 2b,c.

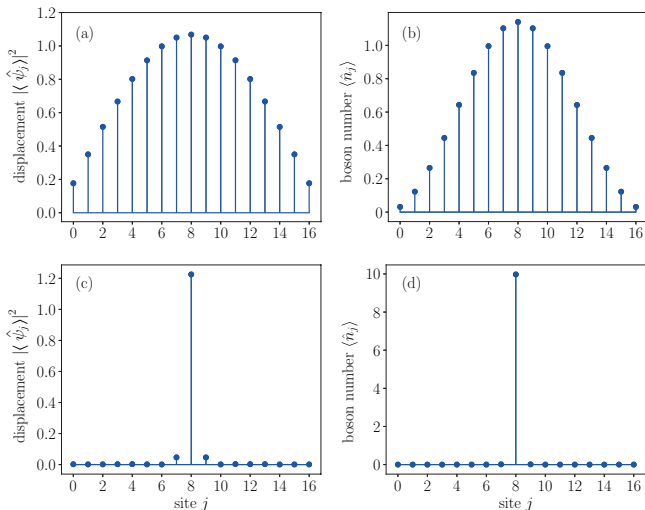


FIG. 2. (a,b) Profile of the ground state for $N_T = 10$ and $\gamma = -0.01$: (a) Square modulus of the expected displacement; (b) expected value of the boson number at different sites; (c,d) as in (a,b) with $N_T = 10$ and $\gamma = -1$ ($n = 17$).

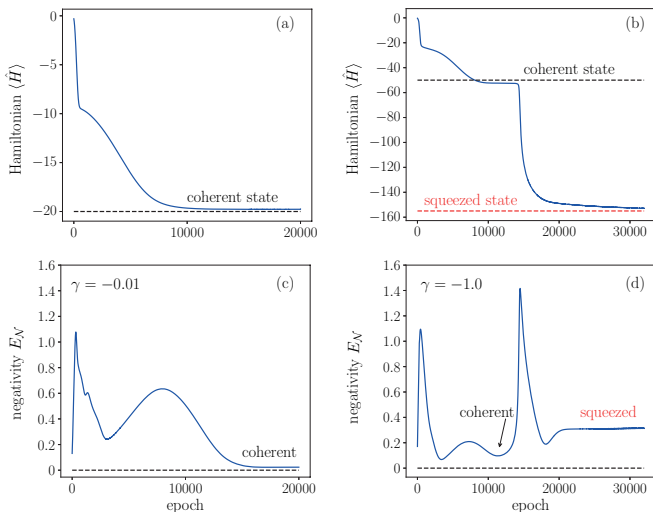


FIG. 3. Training history for the solutions in Fig. 2: (a) $\langle \hat{H} \rangle$ versus the number of epochs, which rapidly reaches the target values for $\gamma = -0.01$; (b) as in (a) for $\gamma = -1$. The NN model explores different plateaus of the Hilbert space, corresponding to discrete solitons with different degree of entanglement; (c) logarithmic negativity during training for $\gamma = -0.01$, no entanglement occurs for negligible interaction; (d) as in (c) for $\gamma = -1$, the lowest energy solution is entangled.

Solutions in Fig. 2 result from the parameter space exploration during training. In figure 3 we report $\langle \hat{H} \rangle$ and $\langle \hat{N} \rangle$ when varying the number of training epochs for $N_T = 10$. The system converges after some thousands of epochs, and during the training the explores different solutions. Figure 3a shows the training of the model when $\gamma = -0.01$: the system converges steadily to the delocalized state in Fig. 2a,b. This can be approximated in the continuum limit, as a non-squeezed coherent state with a sinusoidal profile, and the value of the Hamiltonian $\langle \hat{H} \rangle \simeq -2N_T$, which is approximately the plateau in figure 3a for $N_T = 10$.

Figure 3b shows the strong interaction case $\gamma = -1$. During the training the systems settles in two plateaus $\langle \hat{H} \rangle \cong -50$ and $\langle \hat{H} \rangle \cong -155$. These values are understood in terms of approximate solutions, in which $\langle \psi_{j \neq A} \rangle = 0$, with the exception of central site $A = \lfloor \frac{n}{2} \rfloor + 1$, where the soliton is localized. If we consider the many-body state $|\alpha\rangle = \hat{D}_A(\alpha)|\text{vac}\rangle$ with displacement vector $\alpha_i = \delta_{iA}\alpha$, we have

$$\langle \hat{H} \rangle \simeq \frac{\gamma}{2} \left(\sum_i \langle |\hat{n}_i|^2 \rangle - \langle |\hat{n}_i| \rangle \right) = \frac{\gamma}{2} \sum_i |\alpha_i|^4 = \frac{\gamma}{2} |\alpha|^4 \quad (7)$$

One has $\langle \hat{N} \rangle = |\alpha|^2 = N_T$ and $\langle \hat{H} \rangle = \frac{\gamma}{2} N_T^2$ which gives $\langle \hat{H} \rangle \simeq -50$, approximately the first plateau in Fig. 3. The difference due to the neglected $\langle \hat{K} \rangle$. $|\alpha\rangle$ is a coherent state with negligible entanglement, as detailed below.

The lowest energy asymptotic solution found by the training is obtained at a larger number of epochs is in Fig. 3b. The lowest energy plateau can be estimated by considering a squeezed coherent states obtained as

$$|\alpha, \zeta\rangle = \hat{D}_A(\alpha) \hat{S}_A(\zeta) |\text{vac}\rangle \quad (8)$$

where \hat{S}_A is the squeezing operator for the site $j = A$ with squeezing parameter $\zeta = r e^{i\theta}$. For $|\alpha, \zeta\rangle$ one has

$$\begin{aligned} \langle \hat{N} \rangle &= \sinh(r)^2 + |\alpha|^2 = N_T \\ \langle \hat{H} \rangle &= \frac{5}{8} - 2|\alpha|^2 + |\alpha|^4 + (-1 + 2|\alpha|^2) \cosh(2r) + \frac{3}{8} \cosh(4r) - |\alpha|^2 \cos(2\phi - \theta) \sinh(2r), \end{aligned} \quad (9)$$

with minimum $\langle \hat{H} \rangle \simeq -155$ for $N_T = 10$ as in Fig. 3b. *Entanglement of the single soliton* — Entanglement in Gaussian states can be estimated by the logarithmic negativity [11, 43, 45]. Specifically, we partition the system in a single site “Alice” A at $A = \lfloor \frac{n}{2} \rfloor + 1$ where the soliton is localized. All the remaining sites with $j \neq A$ correspond to “Bob”.

We retrieve the covariance matrix \mathbf{g} from the NN model after training, and compute the partial transpose $\tilde{\mathbf{g}}$ [45], obtained by multiplying by -1 all the matrix elements connected to Alice’s momenta \hat{p}_A . We then compute the symplectic eigenvalues $\tilde{c}_0, \tilde{c}_1, \dots, \tilde{c}_{n-1}$ as the

moduli of the eigenvalues of $\mathbf{J}^\top \tilde{\mathbf{g}}/2$. The logarithmic negativity is

$$E_{\mathcal{N}} = - \sum_{j=0}^{n-1} \log_2 \min\{1, 2c_j\}. \quad (10)$$

Figure 3c shows the trend of $E_{\mathcal{N}}$ for $\gamma = -0.01$ during the training. Despite initially the system explore randomly generated entangled solution, the asymptotic state is a coherent non-squeezed state, with vanishing entanglement as expected for a negligible interaction.

Figure 3d shows $E_{\mathcal{N}}$ during the epochs for $\gamma = -1$, measuring the degree of entanglement of the soliton with the rest of sites. The NN explores the landscape while visiting different states, with varying $E_{\mathcal{N}}$. The local minimum of $\langle \hat{H} \rangle$, is the coherent state with entanglement smaller than the value of the squeezed ground state at epoch 3×10^4 . Nevertheless, the asymptotic value of $E_{\mathcal{N}}$ is negligible if compared with the case of bounded solitons considered in the following.

Entangled solitons — We study bound states of two solitons [28–30]. These can be computed by training the network with proper loss functions. We fix the location of two sites, denoted Alice at A and Bob at $B = A + \Delta$ and we introduce as cost function $\exp(-\langle \hat{n}_A \rangle)$ to maximize the bosons at A and $\exp(\langle \hat{n}_A - \hat{n}_B \rangle)$ to generate a solution with the same boson numbers at A and B .

Figure 4 shows the coupled solitons profiles for different peak positions when $N_T = 40$. At variance with the single soliton in Fig. 2, we find that the expected boson number is not vanishing in all the sites of the array. Nevertheless, the expected value of the intensities $|\langle \psi_j \rangle|^2$ is not vanishing only at the soliton sites, outlining the onset of squeezed nonlocal states in the system.

The found bound soliton solutions are entangled. This can be quantified by considering as a bipartite system composed by the site in A (Alice) and the rest of the sites. As indicated in Fig. 4, the computed $E_{\mathcal{N}}$ depends on the distance Δ between the two solitons. We also find that the logarithmic negativity depends on the number of total bosons N_T : Figure 4c shows $E_{\mathcal{N}}$ versus N_T for various Δ . We observe that the degree of entanglement is small and comparable with the single soliton for case $N_T < 10$, and growing when $N_T > 10$.

Boson sampling — As we show in the following the degree of entanglement is connected to the observation of correlated particles in different output channels.

Boson sampling gives the probability $\text{Pr}(\bar{\mathbf{n}})$ of finding \bar{n}_0 photons in mode 0, \bar{n}_1 photons in mode 1, and so forth, where $\bar{\mathbf{n}} = (\bar{n}_0, \bar{n}_1, \dots, \bar{n}_{n-1})$ is a given photon pattern. Letting $\hat{\rho}$ the density matrix, one has $\text{Pr}(\bar{\mathbf{n}}) = \text{Tr}[\hat{\rho}|\bar{\mathbf{n}}\rangle\langle\bar{\mathbf{n}}|]$, with $|\bar{\mathbf{n}}\rangle\langle\bar{\mathbf{n}}| = \otimes_j |\bar{n}_j\rangle\langle\bar{n}_j|$. Correspondingly [46],

$$\text{Pr}(\bar{\mathbf{n}}) = \frac{1}{\bar{\mathbf{n}}!} \prod_j \left(\frac{\partial^2}{\partial \alpha_j \partial \alpha_j^*} \right)^{\bar{n}_j} e^{\sum_j |\alpha_j|^2} Q_\rho(\boldsymbol{\alpha}) \Big|_{\boldsymbol{\alpha}=0} \quad (11)$$

where $\bar{\mathbf{n}}! = \bar{n}_0! \bar{n}_1! \dots \bar{n}_{n-1}!$ and $Q_\rho = \pi^n \langle \boldsymbol{\alpha} | \rho | \boldsymbol{\alpha} \rangle$ is the Q -representation of the density matrix [40, 41].

We compute $\text{Pr}(\bar{\mathbf{n}})$ as in [47]. For a given bound soliton solution, we consider the probability of observing a number of photons \bar{n}_T in two sites A and B . Specifically, we consider the patterns such that (i) $\bar{n}_A = \bar{n}_B = \bar{n}_T/2$ for $A \neq B$, or (ii) $\bar{n}_A = \bar{n}_B = \bar{n}_T$ when $A = B$, and $\bar{n}_j = 0$ elsewhere. For $\bar{n}_T = 2$ this corresponds to observing a pair of photon in a single site, or two photons in two distinct sites.

Figure 4c shows the pattern probability for $\bar{n}_T = 2$ varying A and B when $N_T = 10$. Such a probability is different from zero only when A and B are the positions of one soliton (located in $A = 3$ and $B = 8$ in the figure). When $A = B$ (yellow bar), we have the probability of observing the two photons in one single soliton. When A and B are the sites of the two solitons (green bar), we have the probability of observing a couple of photons in the two soliton sites. For all other patterns with $\bar{n}_T = 2$ there is a negligible probability of observing a photon pair. Hence, pairs of particles appear either in a single soliton, or as entangled bosons in the two solitons.

Seemingly, when $\bar{n}_T = 4$ we have only non-vanishing probability of observing either 4 bosons in a soliton, or two entangled pairs in the two solitons (Fig. 4d).

Photons are hence observed simultaneously only when they are monitored at the positions of the two localized solitons, demonstrating their quantum correlation and the nonlocality in the system.

Conclusion — Discrete waveguides arrays became popular for a series of experiments concerning the quantum optical advantage in boson sampling. One can argue about the role of nonlinearity, which –in classical regimes– supports discrete self-localized solitons.

For unveiling quantum effects in discrete solitons, we have adopted quantum machine learning. Training of a neural network variational ansatz enables to compute states corresponding to single solitons and their bound states. Specifically, we considered Gaussian states as they are expected to conform to experimental observations at high intensities, and also allow us to rigorously compute the degree of entanglement by the logarithmic negativity. Furthermore, the neural network formulation is compatible with the Gaussian boson sampling protocol and can be used to compute the probabilities of photon patterns toward experimental investigations on the quantum advantage in the presence of nonlinearity.

We found that entangled pairs of photons emerge from self-localized bounded solitons. In addition, the results unveil that properly trained boson sampling circuits can be used to synthesize nonlinear quantum waves. The methodology can be extended beyond Gaussian states, and generalized to continuous systems and multidimensional arrays with arbitrary networks.

We acknowledge support from Horizon 2020 Framework Programme QuantERA grant QUOMPLEX, by

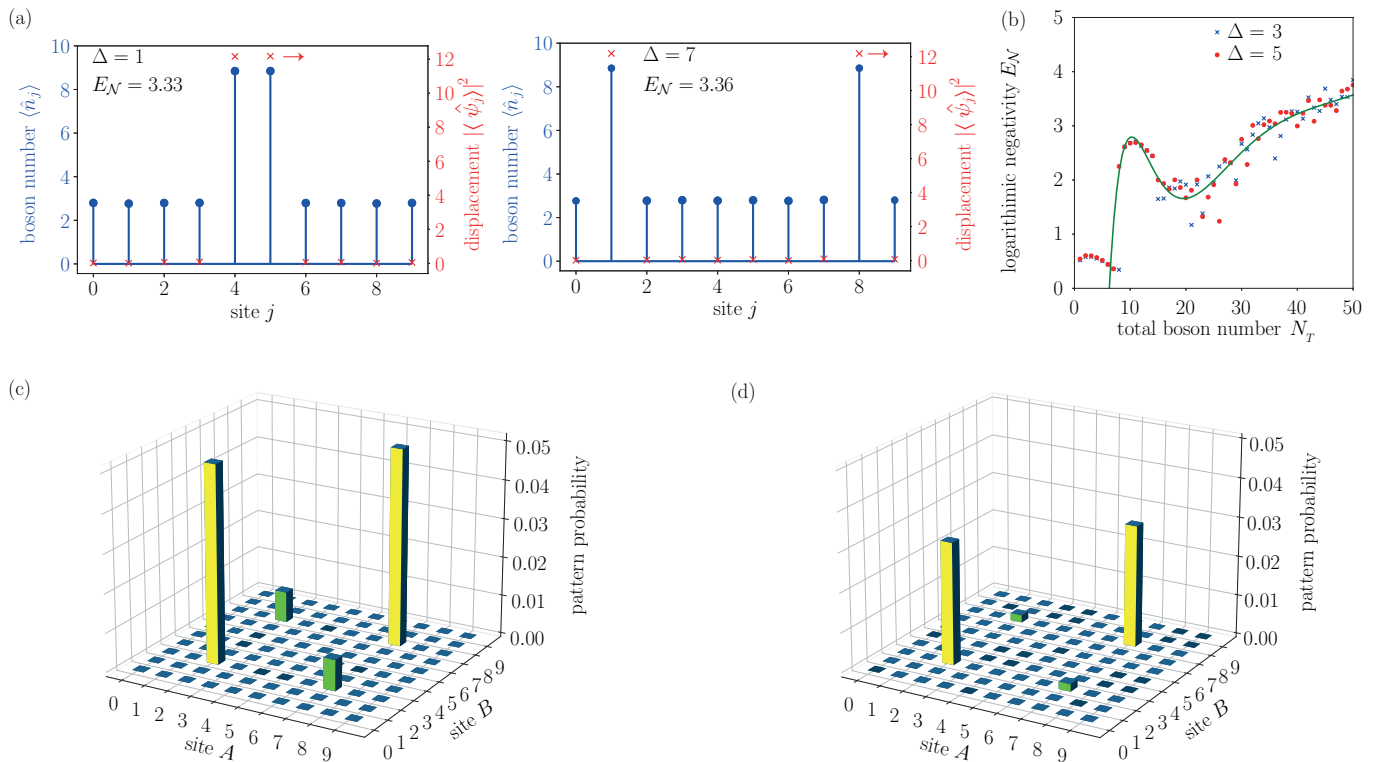


FIG. 4. (a) Boson distribution and mean displacement (right axis) for two representative bounded soliton solutions with $N_T = 40$ and $\gamma = -1.0$; the values of Δ and E_N are reported; (b) logarithmic negativity versus the boson number N_T for different Δ ; (c) boson sampling probabilities for patterns containing $\bar{n}_T = 2$ photons in two varying sites A and B and $N_T = 10$; (d) as in (c) for patterns with 2 photons per site ($\bar{n}_T = 4$). The pattern probability is not vanishing only when the photons in the pattern are at the soliton sites, denoting the generation of entangled pairs ($n = 10$).

National Research Council (CNR), Grant 731473, and H2020 PhoQus project (Grant No. 820392).

* claudio.conti@uniroma1.it

† <https://www.complexlight.org>

- [1] S. R. Friberg, S. Machida, and Y. Yamamoto, Quantum-nondemolition measurement of the photon number of an optical soliton, *Phys. Rev. Lett.* **69**, 3165–3168 (1992).
- [2] P. D. Drummond, R. M. Shelby, S. R. Friberg, and Y. Yamamoto, Quantum solitons in optical fibres, *Nature* **365**, 307–313 (1993).
- [3] C. Silberhorn, P. Lam, O. Weis, F. König, N. Korolkova, *et al.*, Generation of Continuous Variable Einstein-Podolsky-Rosen Entanglement via the Kerr Nonlinearity in an Optical Fiber, *Phys. Rev. Lett.* **86**, 4267–4270 (2001).
- [4] C. X. Yu, H. A. Haus, and E. P. Ippen, Soliton squeezing at the gigahertz rate in a Sagnac loop, *Opt. Lett.* **26**, 669–671 (2001).
- [5] Q.-Y. Liang, A. V. Venkatramani, S. H. Cantu, T. L. Nicholson, M. J. Gullans, A. V. Gorshkov, J. D. Thompson, C. Chin, M. D. Lukin, and V. Vuletić, Observation of three-photon bound states in a quantum nonlinear medium, *Science* **359**, 783 (2018).
- [6] G. Leuchs, T. C. Ralph, C. Silberhorn, and N. Korolkova, Scheme for the generation of entangled solitons for quantum communication, *Journal of Modern Optics* **46**, 1927 (1999).
- [7] R.-K. Lee, Y. Lai, and B. A. Malomed, Generation of photon-number-entangled soliton pairs through interactions, *Phys. Rev. A* **71**, 013816 (2005).
- [8] Y. Lai and R.-K. Lee, Entangled quantum nonlinear schrödinger solitons, *Phys. Rev. Lett.* **103**, 013902 (2009).
- [9] L. D. M. Villari, D. Faccio, F. Biancalana, and C. Conti, Quantum soliton evaporation, *Phys. Rev. A* **98**, 043859 (2018).
- [10] O. V. Marchukov, B. A. Malomed, V. Dunjko, J. Ruhl, M. Olshanii, R. G. Hulet, and V. A. Yurovsky, Quantum fluctuations of the center of mass and relative parameters of nonlinear schrödinger breathers, *Phys. Rev. Lett.* **125**, 050405 (2020).
- [11] V. O. Martynov, V. O. Munyaev, and L. A. Smirnov, Generation of entangled states of light using discrete solitons in waveguide arrays, arXiv:2011.07662 (2020).
- [12] M. J. Potasek and B. Yurke, Squeezed-light generation in a medium governed by the nonlinear schrödinger equation, *Phys. Rev. A* **35**, 3974 (1987).
- [13] Y. Lai and H. A. Haus, Quantum theory of solitons in

- optical fibers. i. time-dependent hartree approximation, *Phys. Rev. A* **40**, 844 (1989).
- [14] E. M. Wright, Quantum theory of soliton propagation in an optical fiber using the Hartree approximation, *Phys. Rev. A* **43**, 3836–3844 (1991).
- [15] A. Scott, J. Eilbeck, and H. Gilhøj, Quantum lattice solitons, *Physica D: Nonlinear Phenomena* **78**, 194 (1994).
- [16] D. Yao, Quantum fluctuations of optical solitons in fibers, *Phys. Rev. A* **52**, 4871–4881 (1995).
- [17] G. Marcucci, D. Pierangeli, and C. Conti, Theory of neuromorphic computing by waves: machine learning by rogue waves, dispersive shocks, and solitons, *Phys. Rev. Lett.* **125**, 093901 (2020).
- [18] R. A. Herrera, Evaluating a neural network and a convolutional neural network for predicting soliton properties in a quantum noise environment, *J. Opt. Soc. Am. B* **37**, 3094 (2020).
- [19] N. A. Silva, T. D. Ferreira, and A. Guerreiro, Reservoir computing with solitons, *New J. Phys.* **23**, 023013 (2021).
- [20] J.-C. Pu, J. Li, and Y. Chen, Soliton, breather, and rogue wave solutions for solving the nonlinear schrödinger equation using a deep learning method with physical constraints, *Chinese Physics B* **30**, 060202 (2021).
- [21] V. Lopez-Pastor and F. Marquardt, Self-learning machines based on hamiltonian echo backpropagation, arXiv:2103.04992 (2021).
- [22] M. Tillmann, B. Dakić, R. Heilmann, S. Nolte, A. Szameit, and P. Walther, Experimental boson sampling, *Nat. Photonics* **7**, 540 (2012).
- [23] M. A. Broome, A. Fedrizzi, S. Rahimi-Keshari, J. Dove, S. Aaronson, T. C. Ralph, and A. G. White, Photonic boson sampling in a tunable circuit, *Science* **339**, 794 (2013).
- [24] J. B. Spring, B. J. Metcalf, P. C. Humphreys, W. S. Kolthammer, X.-M. Jin, M. Barbieri, A. Datta, N. Thomas-Peter, N. K. Langford, D. Kundyś, J. C. Gates, B. J. Smith, P. G. R. Smith, and I. A. Walmsley, Boson sampling on a photonic chip, *Science* **339**, 798 (2013).
- [25] J. Carolan, J. D. A. Meinecke, P. J. Shadbolt, N. J. Russell, N. Ismail, K. Wörhoff, T. Rudolph, M. G. Thompson, J. L. O’Brien, J. C. F. Matthews, and A. Laing, On the experimental verification of quantum complexity in linear optics, *Nat. Photonics* **8**, 621 (2014).
- [26] N. Spagnolo, C. Vitelli, M. Bentivegna, D. J. Brod, A. Crespi, F. Flamini, S. Giacomini, G. Milani, R. Ramponi, P. Mataloni, R. Osellame, E. F. Galvão, and F. Sciarrino, Experimental validation of photonic boson sampling, *Nat. Photonics* **8**, 615 (2014).
- [27] H.-S. Zhong, H. Wang, Y.-H. Deng, M.-C. Chen, L.-C. Peng, Y.-H. Luo, J. Qin, D. Wu, X. Ding, Y. Hu, P. Hu, X.-Y. Yang, W.-J. Zhang, H. Li, Y. Li, X. Jiang, L. Gan, G. Yang, L. You, Z. Wang, L. Li, N.-L. Liu, C.-Y. Lu, and J.-W. Pan, Quantum computational advantage using photons, *Science* **370**, 1460 (2020).
- [28] F. Lederer, G. I. Stegeman, D. N. Christodoulides, G. Assanto, M. Segev, and Y. Silberberg, Discrete solitons in optics, *Physics Reports* **463**, 1 (2008).
- [29] Y. V. Kartashov, B. A. Malomed, and L. Torner, Solitons in nonlinear lattices, *Rev. Mod. Phys.* **83**, 247–305 (2011).
- [30] Y. Kivshar and G. P. Agrawal, *Optical solitons* (Academic Press, New York, 2003).
- [31] G. Carleo, I. Cirac, K. Cranmer, L. Daudet, M. Schuld, N. Tishby, L. Vogt-Maranto, and L. Zdeborová, Machine learning and the physical sciences, *Rev. Mod. Phys.* **91**, 045002 (2019).
- [32] M. Broughton, G. Verdon, T. McCourt, A. J. Martinez, J. H. Yoo, S. V. Isakov, P. Massey, M. Y. Niu, R. Halavati, E. Peters, M. Leib, A. Skolik, M. Streif, D. V. Dollen, J. R. McClean, S. Boixo, D. Bacon, A. K. Ho, H. Neven, and M. Mohseni, Tensorflow quantum: A software framework for quantum machine learning, arXiv:2003.02989 (2020).
- [33] G. Marcucci, D. Pierangeli, P. W. H. Pinkse, M. Malik, and C. Conti, Programming multi-level quantum gates in disordered computing reservoirs via machine learning, *Opt. Express* **28**, 14018 (2020).
- [34] F. Marquardt, Machine learning and quantum devices, arXiv:2101.01759 (2021), arXiv:2101.01759.
- [35] F. Tacchino, S. Mangini, P. K. Barkoutsos, C. Macchiavello, D. Gerace, I. Tavernelli, and D. Bajoni, Variational learning for quantum artificial neural networks, arXiv:2103.02498 (2021).
- [36] A. Kardashin, A. Pervishko, J. Biamonte, and D. Yudin, Numerical hardware-efficient variational quantum simulation of a soliton solution, *Phys. Rev. A* **104**, L020402 (2021).
- [37] H.-Y. Huang, R. Kueng, G. Torlai, V. V. Albert, and J. Preskill, Provably efficient machine learning for quantum many-body problems, arXiv:2106.12627 (2021).
- [38] J. M. Arrazola, V. Bergholm, K. Brádler, T. R. Bromley, M. J. Collins, I. Dhand, A. Fumagalli, T. Gerrits, A. Goussev, L. G. Helt, J. Hundal, T. Isaacsson, R. B. Israel, J. Izaac, S. Jahangiri, R. Janik, N. Killoran, S. P. Kumar, J. Lavoie, A. E. Lita, D. H. Mahler, M. Menotti, B. Morrison, S. W. Nam, L. Neuhaus, H. Y. Qi, N. Quesada, A. Reppingon, K. K. Sabapathy, M. Schuld, D. Su, J. Swinerton, A. Száva, K. Tan, P. Tan, V. D. Vaidya, Z. Vernon, Z. Zabaneh, and Y. Zhang, Quantum circuits with many photons on a programmable nanophotonic chip, *Nature* **591**, 54 (2021).
- [39] F. Hoch, S. Piacentini, T. Giordani, Z.-N. Tian, M. Iuliano, C. Esposito, A. Camillini, G. Carvacho, F. Ceccarelli, N. Spagnolo, A. Crespi, F. Sciarrino, and R. Osellame, Boson sampling in a reconfigurable continuously-coupled 3d photonic circuit, arXiv:2106.08260 (2021).
- [40] C. W. Gardiner and P. Zoller, *Quantum Noise*, 3rd ed. (Springer-Verlag, Berlin, 2004).
- [41] S. M. Barnett and P. M. Radmore, *Methods in Theoretical Quantum Optics* (Oxford University Press, New York, 1997).
- [42] X. Wang, T. Hiroshima, A. Tomita, and M. Hayashi, Quantum information with gaussian states, *Phys. Rep.* **448**, 1 (2007).
- [43] G. Adesso, A. Serafini, and F. Illuminati, Extremal entanglement and mixedness in continuous variable systems, *Phys. Rev. A* **70**, 022318 (2004).
- [44] M. B. Plenio and S. Virmani, An introduction to entanglement measures, *Quantum Inf. Comput.* **7**, 1 (2007).
- [45] G. Vidal and R. F. Werner, Computable measure of entanglement, *Phys. Rev. A* **65**, 032314 (2002).
- [46] R. Kruse, C. S. Hamilton, L. Sansoni, S. Barkhofen, C. Silberhorn, and I. Jex, A detailed study of gaussian boson sampling, *Phys. Rev. A* **100**, 032326 (2019).
- [47] C. Conti, Gaussian boson sampling and multi-particle event optimization by machine learning in the quantum

phase space, arXiv:2102.12142 (2021).